J Mater Sci: Mater Med (2009) 20:1367–1378
DOI 10.1007/s10856-008-3687-8

Fibronectin modulates the morphology of osteoblast-like cells (MG-63) on nano-grooved substrates

Wei-Bor Tsai · Yen-Chung Ting · Jung-Yen Yang · Juin-Yih Lai · Hsuan-Liang Liu

Received: 29 September 2008 / Accepted: 29 December 2008 / Published online: 10 January 2009

Abstract Cell interactions with biomaterials are affected by surface topographic and chemical cues. Although it is well-known that nanometrical grooves/ridges structure modulates cellular spreading, elongation, and alignment, the combinational influence of surface topographic and chemical cues is not well studied. In this study, nano-textured silicon substrata with parallel ridges of 90, 250, or 500 nm wide, separated by grooves with equal width, were fabricated by electron beam lithography and dry etching techniques. Osteoblast-like cells, MG-63, were cultured on the patterned substrata with or without pre-adsorption of fibronectin. The cell morphology was imaged by scanning electron microscopy, and analyzed by image software. We found that FN coating initially modulated cellular spreading, length, and orientation on all types of grooved surfaces. However, after 24 h of culture, the cell morphology was not affected by FN coating on the 250-nm and 500-nm surfaces, while FN decreased cell alignment on the 90-nm surfaces. Our results suggest that surface chemical cues influence the initial cell-substratum contact, while the long-term cellular morphology is dictated by surface topographic cues.

W.-B. Tsai (✉) · Y.-C. Ting
Department of Chemical Engineering, National Taiwan University, No. 1, Roosevelt Road, Sec 4, Taipei, Taiwan
e-mail: weibortsai@ntu.edu.tw

J.-Y. Yang
National Nano Device Laboratories, Hsinchu, Taiwan

J.-Y. Lai
R&D Center for Membrane Technology and Department of Chemical Engineering, Chung Yuan Christian University, Chungli, Taoyuan, Taiwan

H.-L. Liu
Graduate Institute of Biotechnology and Department of Chemical Engineering and Biotechnology, National Taipei University of Technology, Taipei, Taiwan

1 Introduction

In multicellular animals, most of the cells are specialized and cooperatively organized into tissues, which in turn are associated in various combinations to form organs. The extracellular matrix (ECM) helps to hold cells in tissues, and provides an organized lattice within which cells can migrate and interact with one another. The ECM supplies a variety of chemical, topographical, and mechanical cues, that modulate cell morphology, migratory behavior, cellular adhesion, proliferation, differentiation, and apoptosis [1, 2]. For example, epithelial cell sheets reside above a flexible, thin (40–120 nm thick), mat-like ECM—basement membranes, which are consisted of several types of ECM macromolecules including type IV collagen, laminin, entactin, and perlecan [3]. These biomacromolecules provide various bio-signals guiding cellular behavior. For example, laminin possesses the chemical cue to connect epithelial or endothelial cells to the base membrane [4]. Furthermore, the mesh-like structure of basement membranes, consisted of interwound fibers with pores and elevations of nanometric dimensions, provides topographical cues for cell responses [5].

ECM adhesion proteins such as fibronectin (FN), vitronectin, laminin, and collagen provide biochemical signals to mediate cell attachment. A large family of cellular transmembrane receptors, integrins, recognizes these adhesion signals and plays as cellular anchors to dock onto the ECM [6]. One subfamily of the heterodimeric integrins

binds fibronectin and vitronectin with a specific peptide sequence Arg-Gly-Asp (RGD) in these adhesion proteins, while other integrins recognize various peptide sequences. The binding between integrins and their ligands plays a key role in many physiological events, including embryonic development, immune response, leukocyte trafficking, and tumor transfer. Integrin–ligand interactions are also important for in vitro cell culture. In culturing anchorage cells in serum-contained media, serum vitronectin, and fibronectin when adsorbed to the plastic substratum mediate cell attachment on the artificial substrates [7, 8].

Integrins make transmembrane connection between the ECM and the intracellular component—cytoskeleton. The extracellular domain of an integrin is linked to ECM adhesion molecules, while the cytoplasmic domain is linked to stress fibers, which are organized contractile bundles of actin filaments and myosin-II filaments. The ligand-bound integrins first aggregate as clusters at the cell-substratum contact sites, and form small focal complexes that can dynamically disappear or evolve into a specialized sites of adhesion, focal contacts [9, 10]. The integrin complex is linked to actin filament via multiple attachment proteins such as talin and vinculin, and initiates the assembly of cytoskeleton which is composed of actin, myosin, actinin, and tropomyosin. The assembly of actin filaments generates tension that is conveyed to the ECM or the underlying substrata at focal contacts. Cytoskeletal re-organization occurs with progressive spreading of the cells on the substrata to increase attachment strength. One end of a stress fiber is connected to a focal contact and the other end can bind to a second focal contact or a meshwork of intermediate filaments that surrounds the nucleus. Stress fibers would disappear rapidly if tension is released by suddenly detaching one end of a stress fiber from the site of focal contact.

The topography of the ECM is believed to be a critical parameter in guiding cell morphology and migratory behavior in several developmental situations [11]. The fibrillar structure of collagen molecule contributes to the basic topographical feature of the ECM. The basic topographical feature of ECM is composed by collagen fibrils with diameters ranging from 50 to 300 nm, which could assemble into larger cable-like collagen fibers around 1–4 μm in diameter [12]. The alignment of collagen fibers has been shown to be critical for guiding in vivo cell proliferation and migration [13]. The tendency of cells to align, to grow, or to move along a specific orientation defined by some physical properties of substrata, is described as contact guidance [14].

For the past 20 years, cell biologists have systematically investigated cell responses to artificial substrates with well-defined anisotropic micrometric topographies, thanks to the lithographic and dry etching techniques widely used in the microelectronic industry [15]. The most studied topographical features have been parallel grooves/ridges with micrometric dimensions. It has become well documented that many cell types react strongly to micrometric grooves with alteration in many cellular features, such as morphology, orientation, cytoskeleton, and focal contacts arrangement, cellular movement, and gene expression [11, 16, 17]. The most noteworthy feature of cell morphology on grooves/ridges structure is cellular elongation and alignment along the grooves, in contrast to disoriented cellular spreading on flat substrates [11, 18, 19]. Previous studies showed that cells react to the pattern of grooves/ridges with feature dimensions as small as 70 nm in width and 400 nm in pitch spacing [18, 20].

We previously showed that MG-63 cells elongated and aligned on the nano-grooved silicon substrates [21]. However, cell adhesion to the substrates is mainly mediated by the adsorbed serum adhesive proteins from the culture media. This study is aimed to investigate a further question: how cells respond to nano-grooves/ridges under elevated surface concentration of serum adhesion proteins. Fibronectin, the major adhesion protein found in ECM and serum, helps cells to attach to matrix [22], so is selected as the model adhesion protein. In this study, FN was coated to a series of grooved silicon surfaces (groove/ridge widths of 90, 250, and 500 nm; 215 nm in depth) prior to cell adhesion. The dimension of the nano-grooved substrates was close to the dimension of collagen fibrils. The impacts of FN adsorption on the morphology and cytoskeleton arrangement of MG-63 cells were evaluated on these patterned surfaces in a time-dependent manner.

2 Materials and methods

2.1 Fabrication of grooved silicon substrata

Silicon is not ordinarily considered to be a biomaterial as that term is usually used. However, due to its relatively ease of nano-topographic fabrication, grooved silicon substrata were applied in this study. Textured silicon substrates were fabricated by both electron beam (EB) lithography and dry etching techniques [21]. Silicon wafers were cleaned by a standard RCA cleaning procedure [23] which removes organic contaminants, any oxide layer that may have built up, and any ionic or heavy metal contaminants from the wafer surface, followed by a dip in diluted HF solution before being rinsed in deionized water and spin-dried. The wafers were then spin-coated with an EB photoresist and then sequentially patterned by EB lithography. EB exposure was carried out according to target pattern layouts by using Leica Weprint200 stepper. The pattern on the silicon wafer was fabricated by silicon

anisotropic etching in a ratio of 35:125 sccm Cl_2/HBr mixed plasma at a process pressure of 12 mtorr by an inductively coupled plasma system. The EB photoresist on the etched wafer was then removed by an ozone asher. The wafer was cleaned with the mixture of concentrated H_2SO_4 and H_2O_2 (3:1 in volume ratio) at 120°C for 10 min to remove surface organic contamination. Next, the wafer was immersed into an aqueous solution of Buffered Oxide Etchant (a combination of 40% NH_4F and 49% HF in a ratio of 7:1) for 2 min to remove native oxide.

The design of nano-grooved silicon substrates is illustrated in Fig. 1a. The dimensions of the grooves/ridges were determined by scanning electronic microscopy (SEM) and atomic force microscopy using tapping mode (AFM; NanoScope IIIa, Digital Instruments). Figure 1b shows an AFM image of nano-grooves/ridges with 500 nm wide and 215 nm deep. The silicon wafers contained patterned areas with grooves/ridges of different widths (90, 250, and 500 nm) and 215 nm in depth. The patterned areas were separated by flat regions (blank area in Fig. 1a). The patterned wafers were cut with a diamond knife into small chips and then cleaned by immersing in piranha solution (7/3 v/v of 98% H_2SO_4/30% H_2O_2) at 90°C for 20 min, followed by several rinses with deionized water. This procedure removes the oxidized layer on both the groove and the ridge areas. The average surface roughness, determined by AFM, was not found significant change after the chemical treatment (from 0.30 nm to 1.73 nm). Prior to cell culture, the samples were soaked in 70% ethanol overnight and then rinsed twice for 10 min with sterile phosphate buffered saline (PBS; 137 mM NaCl, 2.7 mM KCl, 10 mM Na_2HPO_4, and 1.8 mM KH_2PO_4, pH 7.4).

2.2 Fibronectin purification and adsorption to the patterned surfaces

Fibronectin (FN) was purified from human plasma according to a previous procedure [24]. The plasma first flew through a Sepharose 2B column (Sigma), followed by a gelatin Sepharose 4B column (Amersham). The bound FN was eluted by 6 M urea/TBS solution (0.8 g NaCl and 0.156 g Tris–HCl in 100 ml de-ionized H_2O, pH 7.6). The eluted FN was de-salted and concentrated by centrifugation through a filter (Millipore, UFC910008).

The silicon chips were dipped in 0.1 mg/ml FN/PBS for 60 min and then were rinsed with PBS for 5 min twice. FN absorption to the flat silicon chips was verified by ELISA (enzyme-linked immunosorbent assay). After FN adsorption, the samples were blocked in 1% BSA/PBS for 30 min and then rinsed with PBS. The samples were incubated with rabbit anti-FN polyclonal antibody (1:1000, Sigma) at 37°C for 1 h, and then incubated with horseradish peroxidase conjugated anti-rabbit IgG antibody (1:1000, Sigma) at 37°C for 1 h. Unbound antibodies were rinsed away with PBST (0.05% Tween 20 in PBS) twice. 3,3′,5,5′-tetramethylbenzidine/H_2O_2 was incubated with the samples at room temperature for 10 min. The reaction was stopped by 2 N H_2SO_4, and the absorbance at 450 nm was read in an ELISA reader.

2.3 Cell culture

Osteoblast-like cells (MG-63) were seeded at a density of 5×10^4 cells/well in 24-well TCPS plates containing the silicon chips, and then incubated in Minimum Essential Medium (MEM) with 10% fetal bovine serum at 37°C and 5% CO_2 for a certain period of time. The substrates without FN coating were used as the controls. After the culture media were aspirated, the samples were rinsed with 0.25% glutaraldehyde in PBS, and were then fixed with 2.5% glutaraldehyde for 60 min twice, followed by 1 h of post-fixation in 1% osmium tetroxide. After three rinses with PBS, the samples were then dehydrated in a graded series of ethanol: 30, 50, 70, 80, 90, 95, 100, 100%, and were treated with CO_2 critical point drying. After sputtered with platinum the samples were observed under a scanning electronic microscope (SEM; JOEL, JSM-5310). Six SEM images were captured randomly on each type of substrata for cell morphology analysis.

2.4 Quantification of cell morphology and orientation from the SEM images

The outlines of the cells in the SEM images were traced manually and the enclosed cell areas were quantified by NIH Image J software. The software also fits each cell to a fittest ellipse (Fig. 2). The lengths of the major and the minor axes of the fittest ellipse represent cell length and width in this study, respectively. Elongation, describing the extent of cell stretch, is the quotient of the major axis divided by the minor axis. Orientation, which is described by the angle between the major axis of the fittest ellipse and the grooves, represents the alignment of an individual cell along the aspect of grooves. The cell of which orientation angle is smaller than 10° is defined as "alignment with groove direction" according to the alignment criterion suggested by Clark et al. [11].

2.5 Fluorescence staining of F-actin, vinculin, and nuclei

After cell culture, the samples were fixed by 4% paraformaldehyde for 15 min and then permeated with 0.1% Triton X-100 in 50 mM glycine for 10 min, followed by two rinses with PBS. The samples were blocked in 2.5% BSA solution for 20 min before staining. F-actin was

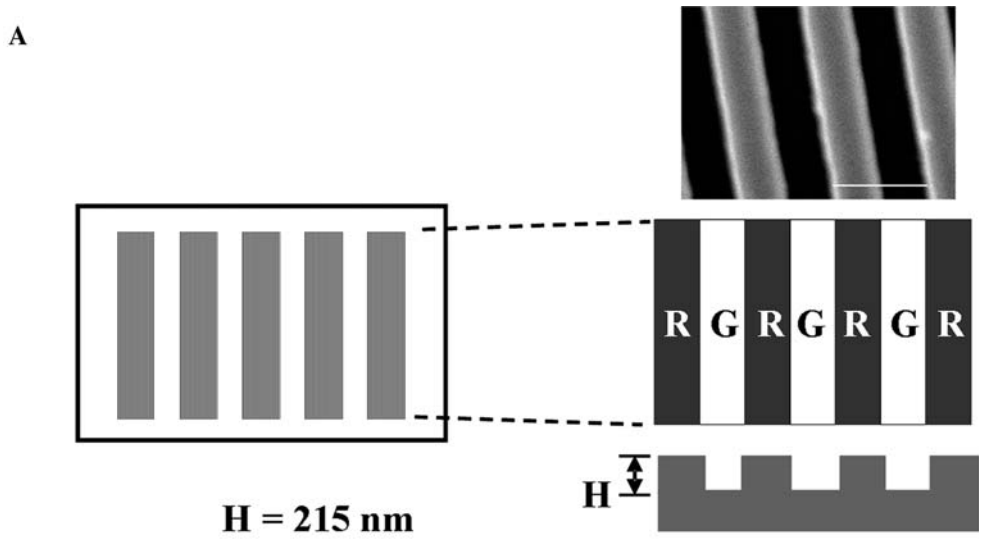

	1	2	3
R (nm)	90	250	500
G (nm)	90	250	500

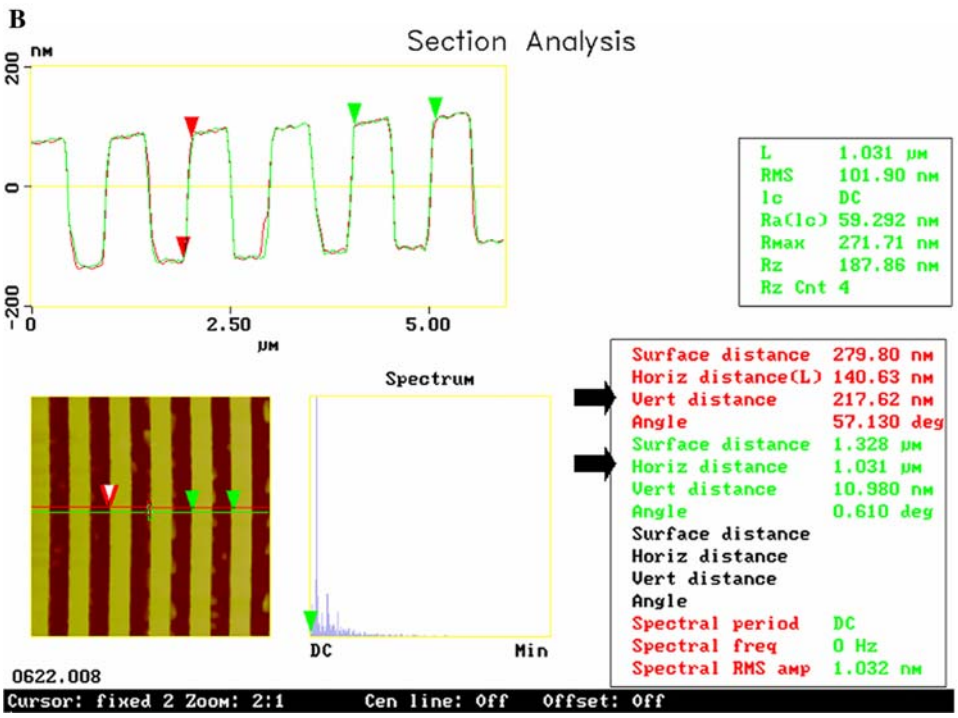

Fig. 1 **a** Design of the nano-grooved silicon substrates. Each chip consisted of an array of 300 µm wide and 1 cm long stripes of patterned fields, separated by smooth areas. The patterns in each field are consisted of ridges (R) and grooves (G) with equal widths which are listed in the figure. The depth (H) of the grooves was approximately 215 nm, determined by atomic force microscope. An example of SEM images of the nano-grooved surfaces (500 nm) is shown on the top-right corner. Scale bar = 1 µm. **b** An AFM image of nano-grooves/ridges with 500 nm wide and 215 nm deep. The measured depth and period of the pattern were listed in the lower right box and indicated by the arrows

stained with 500 nM phalloidin-TRITC (Sigma) for 30 min. Vinculin was first recognized by anti-vinculin monoclonal antibody (Sigma; 200× dilution in 1% Triton X-100 in PBS) for 60 min at 37°C, followed by labeling with anti-mouse IgG-FITC antibody (Sigma; 90× dilution in 1% Triton X-100 in PBS) for 60 min at 37°C. Cell nuclei were stained with 100 nM DAPI (Invitrogen) for 30 min. The fluorescent images were taken with a confocal spectral microscopy (Leica TCS SP2). Excitation wave lengths were 488 nm for both TRITC and FITC, and

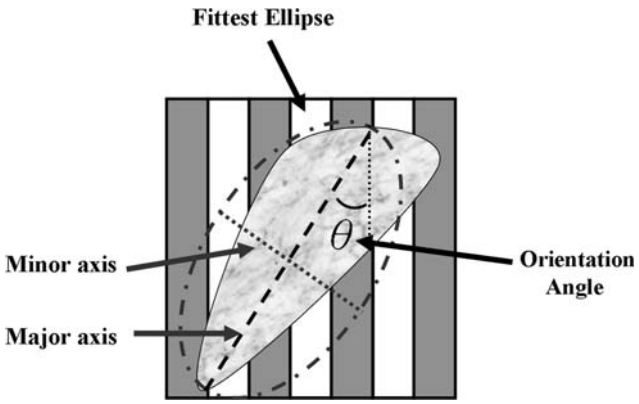

Fig. 2 Schematic of characteristic parameters of cell morphology. The ellipse in dashed line represents the fittest ellipse of cell shape, determined by software Image J. Elongation is given from dividing the length of the major axis of the fittest ellipse by the length of the minor axis. Orientation angle is obtained from the angle between the direction of the underlying grooves and the major axis of the fitted ellipse

400 nm for DAPI, while emission wavelengths were 577–700 nm for TRITC, 520 nm for FITC, and 430–460 nm for DAPI.

2.6 Statistics

All statistical data were performed with the GraphPad InStat software (GraphPad Software, USA). Statistical significance is obtained from Student's *t*-test and ANOVA. The *P* values less than 0.05 were considered significant.

3 Results

FN adsorption to the silicon substrates was verified by ELISA. The absorbance for the FN-coated substrate (0.075 ± 0.002, $n = 4$) was significantly higher than those for the substrate pre-incubated in cell culture medium (0.045 ± 0.001) and the blank sample (0.044 ± 0.000) ($P < 0.001$). The results indicated that pre-adsorption of FN increased the amount of surface-bound FN on the silicon substrates.

The impact of FN adsorption on the morphology of MG-63 cells on the grooved surfaces was first observed by using SEM. After 2 h of incubation, the cells on the surfaces pre-coated with FN spread more than the controls. Figure 3a shows that most of the cells attached to the control flat surface remained spherical morphology after 2-h culture, while many cells already spread out on the FN-coated flat silicon substrate (Fig. 3b). Similar phenomenon was found on the nano-grooved surfaces (Fig. 3c–f). Besides, there were more spread and elongated cells on the control nano-grooved surfaces than the control flat surface (comparing Fig. 3c, e to a). Furthermore, cells were less aligned on the FN-coated grooved substrates compared to the control ones (comparing Fig. 3c, e to d, f, respectively). After 8 h of incubation, most of the cells spread out on all types of substrates. While the cells cultured on the flat surfaces displayed random orientation, the cells cultured on the nano-grooved surfaces became elongated and aligned morphology along the ridges. Figure 3g shows that many cells on the control 90-nm surface were in an ellipse shape and were aligned in a direction, but with FN coating cells seemed to be less aligned (Fig. 3h). However, on the 250 and 500-nm surfaces, the impact of FN seems less obvious (Fig. 3i, j). After 24 h, most of the cells on the 250-FN and 500-FN surfaces were elongated and aligned with the ridges (Fig. 3k), while there were still considerable dis-oriented cells on the 90-FN surface (Fig. 3l).

The cell morphology was further analyzed by five parameters: cell length, cell width, cell area, elongation, and orientation. After 2-h incubation the cells on the FN-coated surfaces exhibited longer morphology compared to the controls with the same topographical features (Fig. 4A). The cell length was also increased with increasing ridge widths. The enhancement of FN on cell length was diminished with time. After 8 h of incubation, the cell lengths at the control substrates were increased to a level comparable to the FN-coated substrates. After 24 h of culture, the cell lengths were only dependent on the dimensions of the patterns: 500 nm > 250 nm > 90 nm > flat, but not on FN coating.

The 2-h cell widths on the control 250-nm and 500-nm surfaces were significantly lower than those on the control flat and 90-nm surfaces (Fig. 4B). Similar to the trend for cell length, FN enhanced initial cell width, while the cells were still wider on the flat and the 90-nm surfaces than the 250-nm and 500-nm ones. The cell widths on the grooved surfaces were decreased with time. After 24 h of culture, the cell widths on the 250 and 500 nm surfaces were not affected by FN coating, but the cell width on the 90-nm substrates was still enhanced by FN coating ($P < 0.05$).

FN coating greatly enhanced initial cell spreading on all the types of substrates (Fig. 4C). After 2 h of culture, the average spreading areas of the cells on the FN-precoated grooved surfaces were more than 350 μm^2, while those on the controls were only about 200 μm^2. After 8 h of culture, the spreading areas on the FN-coated surfaces were still higher than those on the corresponding control substrates, but the difference was decreased. After 24 h of incubation, the cell spreading areas on the control grooved surfaces were regardless of FN coating.

Cell elongation is the ratio of cell length to cell width. After 2 h of incubation, cell elongation was increased with increasing groove widths, and cell elongation was not affected by FN coating (Fig. 4D). Cell elongation was

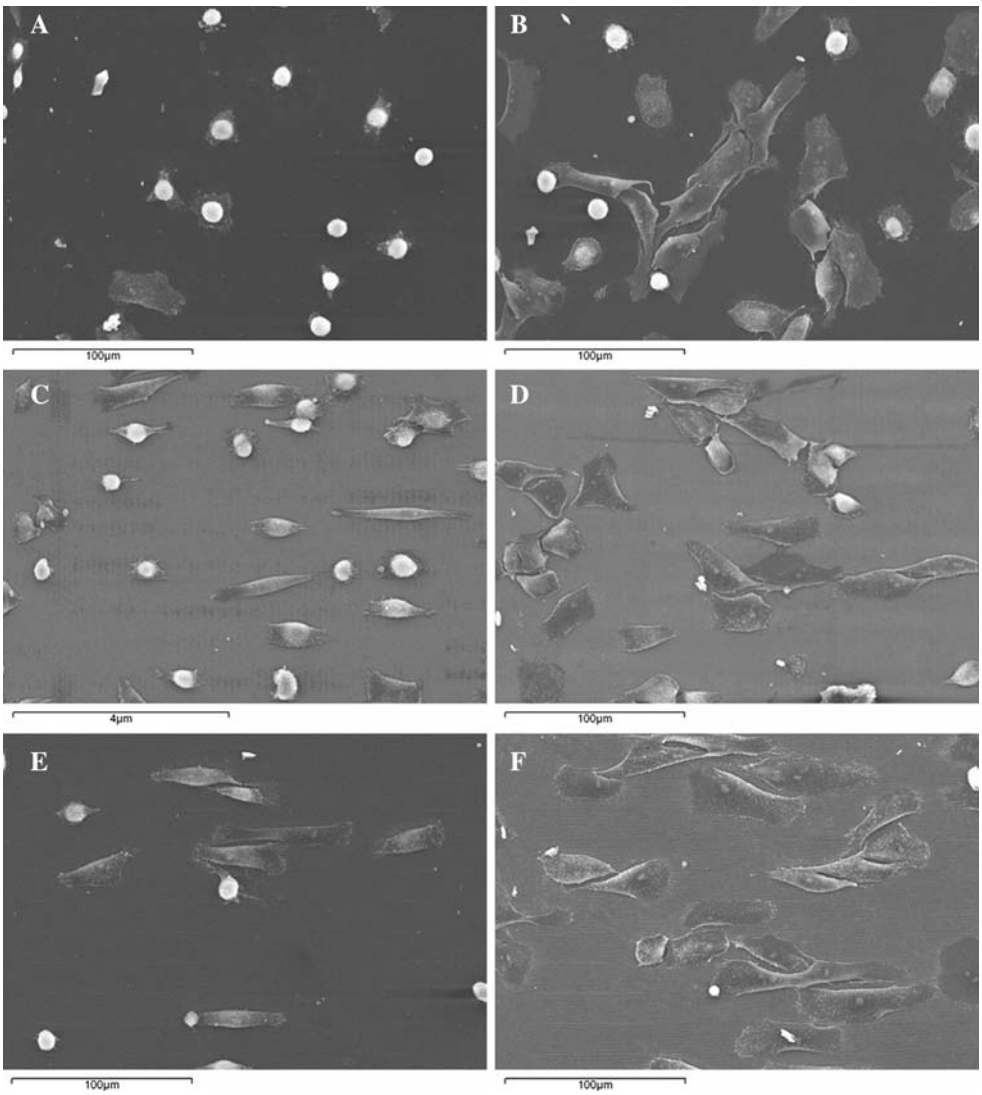

Fig. 3 Scanning electron micrographs of MG-63 cells on the flat or grooved silicon surfaces. The condition in each image is indicated by surface type—FN adsorption—incubation time: **a** Flat: 2 h; **b** Flat–FN: 2 h; **c** 90 nm: 2 h; **d** 90 nm–FN: 2 h; **e** 500 nm: 2 h; **f** 500 nm–FN: 2 h; **g** 90 nm: 8 h; **h** 90 nm–FN: 8 h; **i** 500 nm: 8 h; **j** 500 nm–FN: 8 h; **k** 90 nm: 24 h; **l** 90 nm–FN: 24 h. The scale bars represent 25 μm, except in L (10 μm). The direction of the ridges/grooves in C–J and L is horizontal, while that in K is indicated by the *arrow*

increased with time on all the grooved surfaces, but the increasing rates were smaller on the FN-coated 90 and 250-nm surfaces than those on the controls. After 24 h of incubation, no significant difference in cell elongation was found between the FN-coated and the control substrates. Our results indicate that FN coating exerts little effect on cell elongation.

Cell alignment on the grooved substrates was evaluated by two parameters: average orientation and proportion of the aligned cells. The average cellular orientation on the flat surfaces was around 45°, indicating no preferred orientation no matter whether FN was coated or not (Fig. 5A). On the other hand, cell alignment was apparent on all the nano-grooved surfaces ($P < 0.001$ vs. the flat substrate). FN coating seemed to enhance initial alignment on the 250-nm and 500-nm surfaces, but retarded cell alignment on the 90-nm surface. Furthermore, cell alignment was improved with time on the grooved surfaces. For most of the grooved surfaces, the average cell orientations were decreased to less than 10° after 24 h of incubation, except on the 90-nm FN surface. The final cell orientation on the 90-nm surface was apparently lessened by FN coating ($P < 0.05$ vs. the control 90-nm surface). We also counted the proportion of aligned cells (<10°) on the grooved surfaces (Fig. 5B). Since the cells cultured on the flat surface did not show any preferred direction, we did not calculate the proportion of aligned cells on the flat surface. The population of oriented cells was enhanced by increasing groove widths after 2-h culture, and was increased with time on all the substrates. After 8 h of incubation, the fraction of the aligned cells was much lower on all the FN-coated surfaces compared to their controls. It is noteworthy that the MG-63 cells maintained less oriented population on 90-nm FN surface than on the other wider ridges. After 24 h of incubation, only ~50% of the cells on the 90-nm FN surface were aligned along the direction of grooves, in contrast to over 70% on the other substrates.

Fig. 3 continued

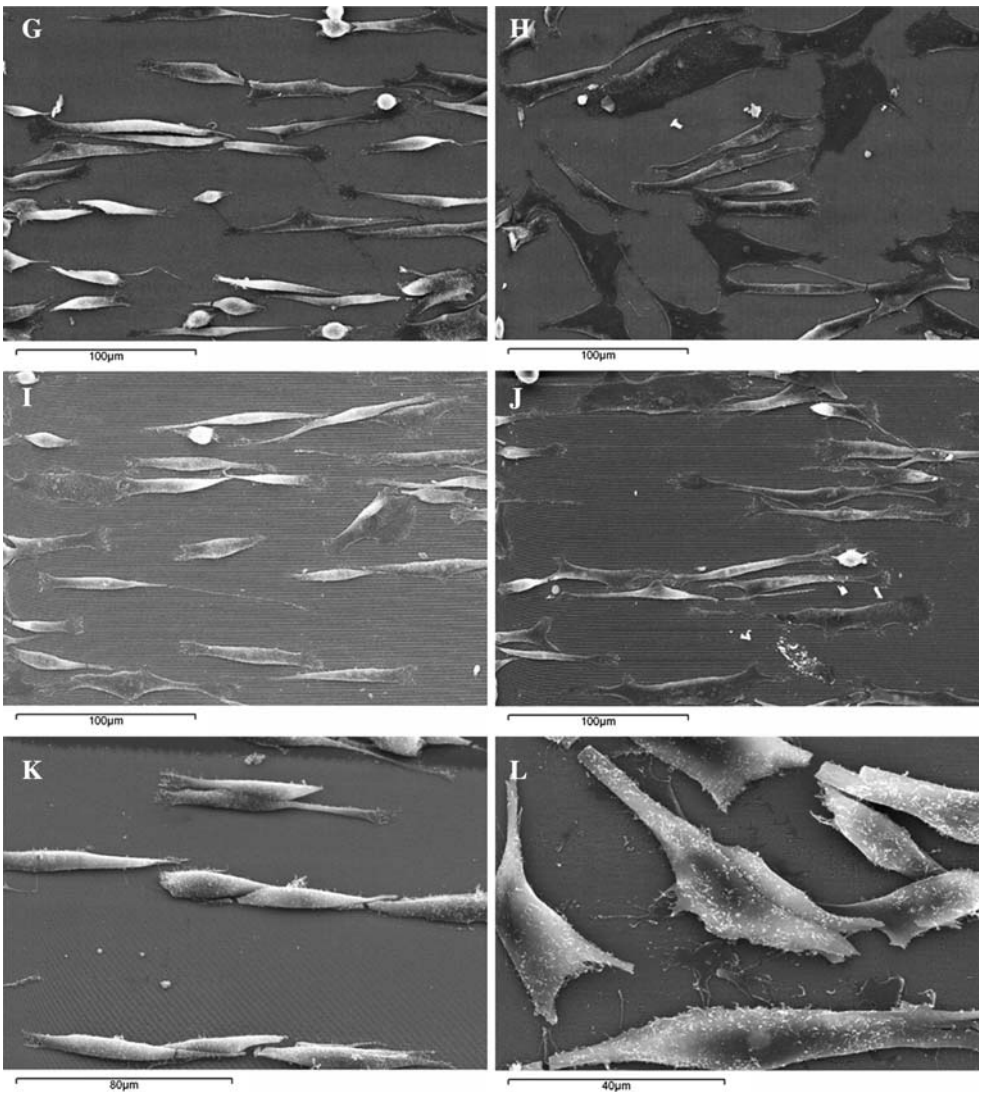

We next examined the formation of actin filaments and focal contacts inside the cells cultured on the patterned substrates. After 2 h of incubation, the formation of actin filaments was not apparent yet. After 4 h, actin filaments were still not clear on the control 90-nm surface (Fig. 6a), while visible actin filaments and focal contacts were established on the 90-nm FN surface (Fig. 6b, c). The locations of the focal contacts were superimposed on the actin filaments. Similarly, actin filaments and focal contacts were formed in the cells cultured on the 250 and 500 nm surfaces precoated with FN (Fig. 6d, e).We found that the actin filaments formed on the 90-nm FN surface were thinner than those formed on the F-FN surface, 250-nm FN and 500-nm FN substrates. Furthermore, most of the actin filaments on the 500-nm surface was aligned with the ridge direction (Fig. 6d). On the other hand, it is interesting to note that on the 90-nm FN surface, some cells possessed unaligned actin filaments (the star sign in Fig. 6b), and some cells possessing aligned actin filaments did not orient along the ridge direction (the triangle sign in Fig. 6b). After 24 h most cells cultured on the smooth substrates and on the patterned surfaces displayed larger stress fibers (Fig. 6f, g). We found that most of the cells on the 90-nm FN substrates displayed aligned actin filaments at that time, but the actin filaments were still thinner than those on the flat and the other nano-grooved surfaces.

Nucleus deformation could be induced by micro-grooved surfaces and has been linked to changes in gene expression [25]. It is suggested that the tensile forces causing cell elongation can also be imparted to the nucleus through the actin-intermediate filament system, and cause nucleus deformation [26]. From the fluorescent images of the nuclei, the cells cultured on the nano-grooved surfaces possess more elongated and oriented nuclei than those on the flat surface (Fig. 7a, b). The nuclei on the flat surface did not have any preferred orientation and did not extend as

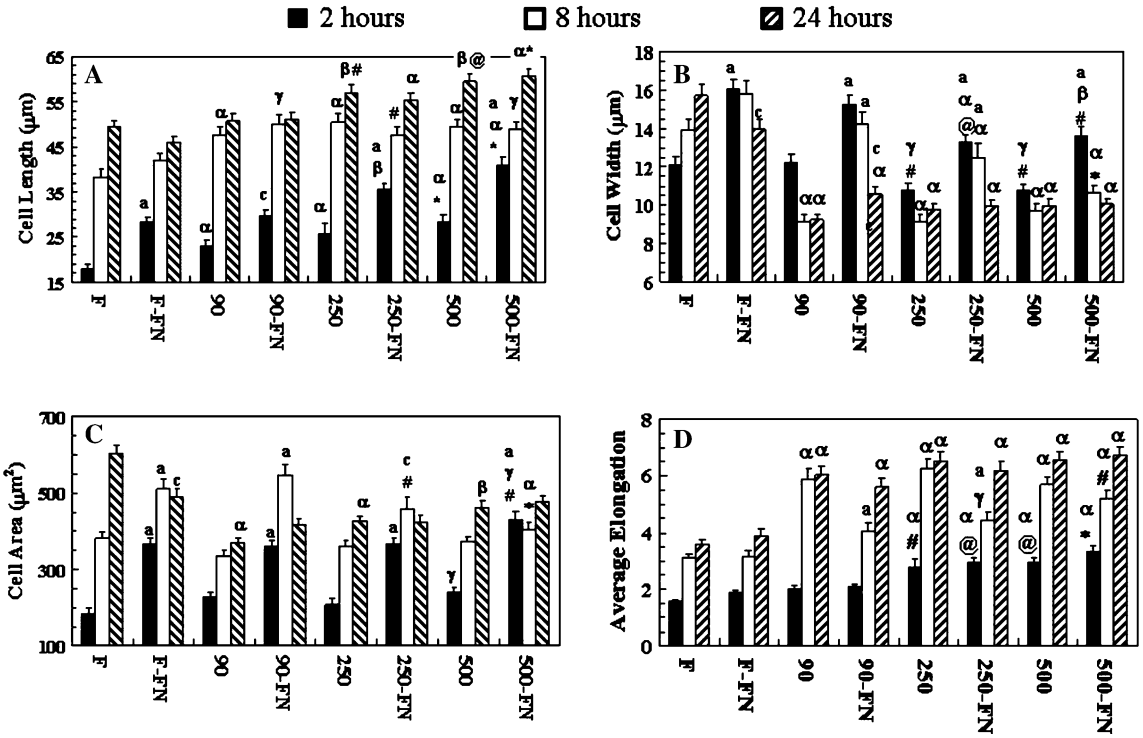

Fig. 4 Quantitative analysis of the morphology of MG-63 cells cultured on the flat and the grooved substrata: **A** cell length, **B** cell width, **C** cell area and **D** average elongation. The data are presented as mean ± standard error of the mean, $n = 57$–124. This experiment has been repeated three times. The symbols for statistical significance: $^{a}P < 0.001$; $^{b}P < 0.01$; and $^{c}P < 0.05$ compared with the controls without FN coating at the same incubation time; $^{\alpha}P < 0.001$, $^{\beta}P < 0.01$ and $^{\gamma}P < 0.05$ compared with the corresponding flat surfaces at the same incubation time; $^{*}P < 0.001$, $^{@}P < 0.01$ and $^{\#}P < 0.05$ compared with the corresponding 90-nm surfaces at the same incubation time

large as those on the patterned substrates (Fig. 7c, d). Nevertheless, the difference in orientation and elongation between the FN-coated and the control grooved substrates was not significant after 24 h of incubation.

4 Discussion

Both topography and chemistry of the substrate affect cell behavior, so it is critical to ascertain whether the surface chemistry in the grooves and on the ridges is similar before we interpret the effects of nano-grooved structures and adhesive proteins on cell adhesion. In this study, the oxidized silicon surfaces in both groove and ridge regions were removed by piranha solution prior to cell experiments. We expect that the same level of oxidation will be developed on both regions afterwards. Thus, similar surface chemistry (oxidized silicon) will be created on the groove and ridge surfaces.

Previous studies on micro-grooved surfaces show that the most notable impacts on cell morphology are inhibition of cellular lateral expansion across the grooves and promotion of marginal expansion on the ridges [27]. Similar tendency was found on the nano-grooves/ridges structures used in this study (Fig. 4a, b). Since thick actin filaments were not found after 2 h of incubation, initial cell width may reflect the probability of cellular traversing the grooves. The 2-h cell widths on the flat and the 90-nm surfaces were similar, suggesting that the 90-nm gaps do not hamper initial cellular lateral expansion. On the other hand, the cell widths on the 250-nm and 500-nm surfaces were significantly smaller than those on the flat and 90-nm surfaces at that time, showing that the gaps over 250 nm act as effective trenches for reducing cellular lateral extension. An increase in surface FN concentration provides more integrin anchorage sites for lamellipodia to traverse grooves, so the cell widths are enhanced on all the grooved substrates by FN coating. Nevertheless, even with FN coating the cells were still narrower on the 250 nm and the 500 nm surfaces than on the flat and 90-nm surfaces. Similarly, FN coating also increases the cell length (Fig. 4a). As a result, cell spreading area is greatly enlarged by FN coating (Fig. 4c). It is interesting to note that cell elongation on a substrate was little affected by FN coating at 2 h (Fig. 4d), suggesting that FN bolsters up initial cellular expansion in both directions to a similar extent.

After initial cell attachment, the cells are transformed with time: decrease in cell widths and increase in cell

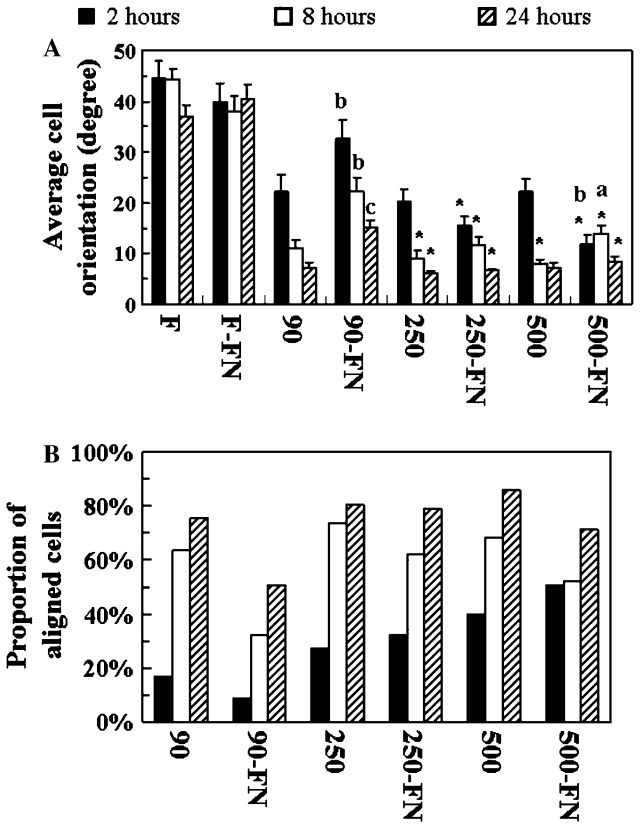

Fig. 5 Cellular alignment. **A** Average cell orientation: the angle between the major axis of the fittest ellipse and the grooves. The data in Fig. 5A are presented as mean ± standard error of the mean, $n = 57$–124. $^{a}P < 0.001$, $^{b}P < 0.01$ and $^{c}P < 0.05$ compared with the controls without FN coating at the same incubation time; $^{*}P < 0.001$, $^{@}P < 0.01$ and $^{\#}P < 0.05$ compared with the corresponding 90-nm surfaces at the same incubation time. **B** The proportion of aligned cells: when the angle between the directions of the major axis of the fittest ellipse of a cell and of the grooves is smaller than 10°, the cell is defined as "align" with the grooves. Cells did not show any preferred orientation on flat substrates, the data for the percentage of aligned cells on the flat surfaces are not included

lengths. The time-dependence of cell morphological transition could be explained in terms of re-organization of focal contacts and intracellular cytoskeleton [28]. It is generally thought that focal contacts are mainly confined on the ridges of micro-grooved surfaces, especially narrow grooves (<2 μm) which cells cannot penetrate in [29, 30]. On the other hand, grooves prevent the formation of stable focal contacts and stress fibers in the direction perpendicular to the ridges. Therefore, focal contacts, actin microfilament bundles and microtubules have found to align on the ridges [19, 31]. The direction generated by the actin filaments are correspondent to the long axis of focal contacts [32]. Similarly, the anisotropic formation of the actin filaments on the nano-grooved surface generates stronger tension in the direction parallel to the ridges than in the perpendicular direction. Thus, the tug-of-war between the two orthogonal forces leads to the elongation of stress fibers along the ridges and the withdrawal of lamellipodia from the lateral edges (Fig. 8).

The transition of cell morphology depends on the dimensions of grooves/ridges and the surface FN concentrations. Cellular elongation and alignment along the direction of grooves/ridges is determined by several topographic parameters such as ridge width, groove width, groove depth, and pattern frequency [33]. The impact of the ridge width on cellular elongation and alignment might be related to the organization of focal contacts and stress fibers. Several studies have shown that the measured width of the focal contacts is dictated by the ridge widths on the underlying substrata [18, 28, 34]. Focal contact plaques are proposed as elongated structures of 0.25–0.5 μm wide and 2.0–10.0 μm long [34]. When the sizes of ridges are close to or less than the width of focal contact plaques, the formation of mature focal contacts and stress fibers is retarded [18]. A previous study also showed that stress fibers were abundant on the cells cultured on the microscale patterns but were rare on 70 nm wide ridges with a 400-nm pitch [18]. We found that the actin microfilaments formed on the surface with 90-nm ridges, which are smaller than the widths of focal contacts, were obviously thinner than on the flat surface and the wider patterns. We suggest that the retardation of the formation of actin filaments on the 90-nm ridges without FN coating renders smaller cell elongation than on the 250-nm and 500-nm surfaces initially.

Similarly, cell alignment with the grooves/ridges is induced by the formation of focal contacts and actin filaments along the ridges. It has been proposed that the narrow strips of substrata limit the orientation of the long axe of focal contacts and induce their alignment, thus influencing the local direction of cell spreading [34]. It is previously suggested that ridge width accounts for ~90% of cellular alignment response [27]. On the patterns with ridges of 250 nm in width and wider, approximately 70% of keratocytes were aligned along the patterns compared to only 45% on a substrate with 70-nm ridges after 12 h of incubation [18]. We also found that higher percentages of MG-63 cells were aligned on the wider ridges than on the 90-nm surface after 2 h of incubation, although the difference was diminished after 8 h of incubation. Apparently, the formation of thinner actin filaments on the 90-nm surfaces delays cell alignment. From the observation in these two studies, cell alignment is retarded on the ridge dimensions less than 100 nm. Therefore, the ridge widths determine cellular alignment.

An increase in FN adsorption enhances the total amount of integrin–ligand bonds, and thus cell–substrate interactions. The increased density of integrin-FN binding is likely to facilitate formation of focal contacts and stress fibers, and thus influences the time-dependent changes in

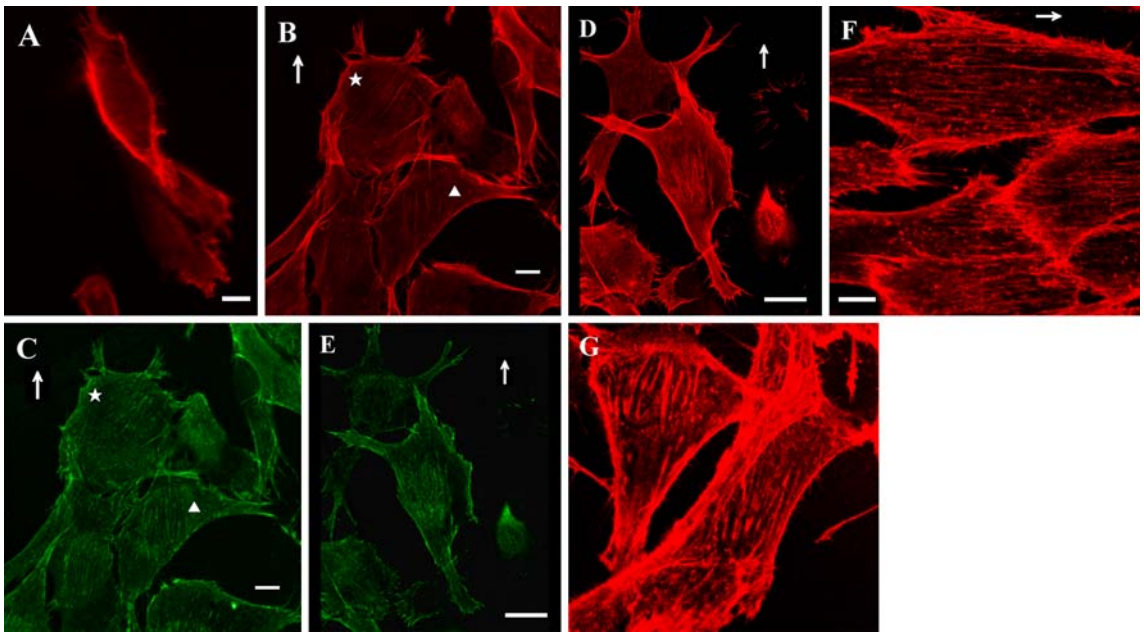

Fig. 6 The cytoskeleton development in the MG-63 cells cultured on the flat and grooved surfaces. Actin filaments (AF) were stained by phalloidin-TRITC (red), vinculin (VN) was immuno-stained by anti-vinculin monoclonal antibody and FITC-conjugated anti-mouse IgG antibody (green). The condition in each image is indicated by surface type—FN adsorption—incubation time—image types: (**a**) 90 nm—4 h—AF; (**b**) 90 nm—FN—4 h—AF; (**c**) 90 nm—FN—4 h—VN; (**d**) 500 nm—FN—4 h—AF; (**e**) 500 nm—FN—4 h—VN; (**f**) 90 nm—FN—24 h—AF; (**g**) Flat—FN—24 h—AF. The scale bars represent 10 μm (**a**, **c**, and **f**) or 20 μm (**b**, **d**, **e**), and the arrows indicate the direction of grooves/ridges

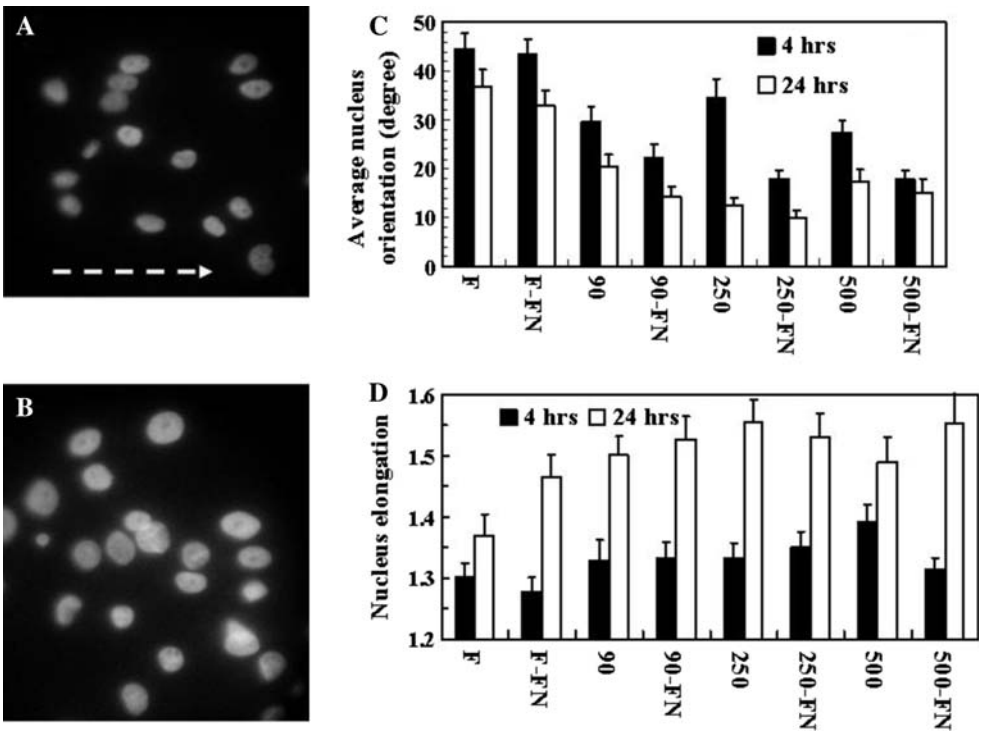

Fig. 7 Morphology of cell nuclei. **a** The fluorescent image of cell nuclei on the 500 nm FN surface and **b** the fluorescent image of cell nuclei on the flat-FN surface after 24 h of incubation; **c** the average angles between the directions of nuclei and the grooves and **d** nucleus elongation. The data present as mean ± standard error of the mean, $n = 50$–80

cellular morphology. The most profound impact of FN coating found in this study is to delay cell lateral retraction (Fig. 4c). The cell widths on the control grooved surfaces were reduced to a minimum about 10 μm after 8 h of incubation, while the duration for reducing cell widths to this value is prolonged on the FN-coated grooved surfaces,

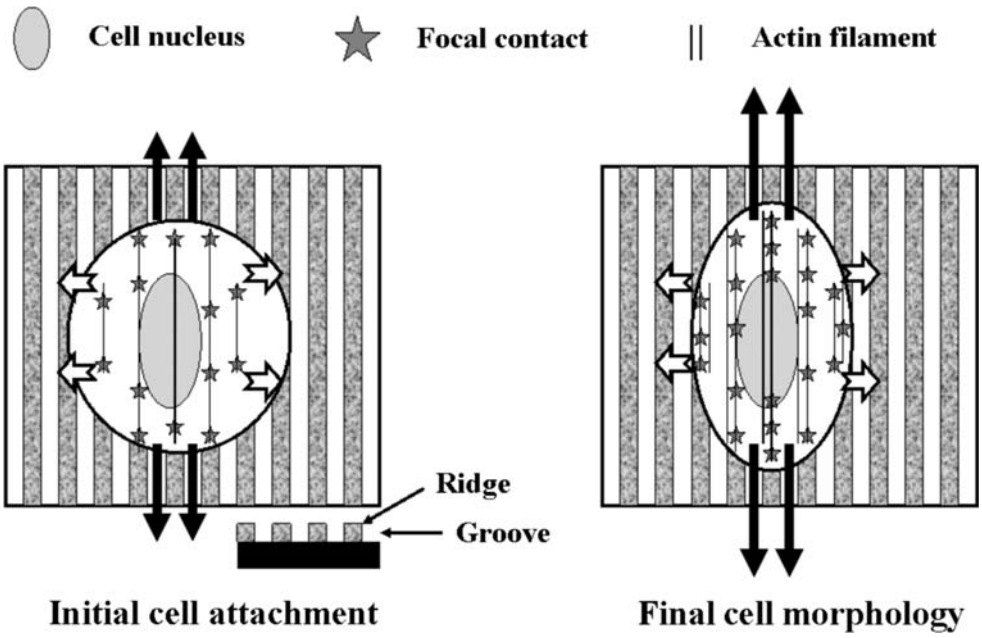

Fig. 8 The schematic presentation of the mechanism of cellular morphologic changes on grooved surfaces

depending on ridge widths. Cellular lateral retraction was not delayed on the 500-nm FN surfaces, while cell widths on the 90-nm FN and 250-nm FN surfaces were still much larger than the minimal values after 8 h of incubation. The retraction of lateral lamellipodia may depend on two counter forces: the tension generated by the stress fibers on the ridge (solid arrows in Fig. 8), which extends the major axis of the cells, and the attachment force of focal contacts to the substrates on the lateral lamellipodia (open arrows in Fig. 8), which maintains cell width. The increased integrin–FN binding might increase the formation of stable focal contacts, and thus the cell–substrate attachment strength. It is reported that the magnitude of the force generated by the actin filaments are correspondent to the size of the mature focal contacts [32]. Therefore, the force generated on the 500-nm surface should be larger than those on the 90-nm and 250-nm surfaces, resulting in quicker retraction of the lateral lamellipodia on the 500-nm substrate. On the other hand, the tension generated on the 90-nm surface may be not enough to counteract on the increased lateral attachment forces due to FN coating. Thus, we found that the cell width on the FN-coated 90-nm surfaces was still higher than that on the control after 24 h of incubation. Nevertheless, we cannot exclude the role of grooves acting as barriers to inhibit cellular lateral expansion. It is generally expected that the difficulty in traversing grooves would be enhanced with increasing groove width [27]. Therefore, the 500-nm gap is less favorable for cellular lateral expansion than the smaller gaps, which may partly contribute to the quick lateral retraction on the 500-nm surface. Nevertheless, the actual cellular mechanism for the FN-induced changes in cellular morphology needs more investigation.

Similarly, FN coating affects cell alignment most significantly on the 90-nm surfaces. Cell alignment was decreased on the 90-nm surfaces by FN adsorption, while cell alignment on the 250-nm and 500-nm substrates was not affected by FN coating after 24 h of culture. The disorientation of C3A cells on the 90-nm substrate might be due to weak stress fibers on such small ridges. As observed in Fig. 6b, c, although FN enhances the formation of focal contacts and actin filaments on the 90-nm substrate, some cells formed unaligned actin filaments, and some cells with aligned actin filaments did not exhibit morphology complying with the ridge direction. Such phenomenon was seldom found on the 250-nm FN and the 500-nm FN surfaces. Similar to the reasoning in cell elongation, the force generated by the thin actin filaments on the 90-nm surface may be not enough to orientate cells when the cell-substratum contacts are enhanced by increased FN surface concentration.

5 Conclusion

Understanding the surface chemical and topographic features that influence cell adhesion and alignment is of great importance not only for developmental biology, but also for cell-based biomedical devices and tissue-engineered products. This study shows that both surface topographical and chemical cues modulate cell morphology and orientation. The chemical cues merely influence the initial

cell-substratum contact, while the long-term cellular morphology is dictated by the surface topographic cues. Our results might reflect the mechanism of cell arrangement in tissue and organs. The adhesive signals, such as fibronectin and laminin, are responsible for facilitating initial cell attachment, while the topography of ECM woven by collagen fibers decides the cell morphology.

Acknowledgment The authors gratefully acknowledge financial support from National Science Council, Taiwan (93-2214-E-002-035). The authors also thank Ms Chia-Hua Lin for manuscript preparation.

References

1. M. Nakamura, T. Nishida, Cornea **18**, 686 (1999). doi:10.1097/00003226-199911000-00011
2. D.K. Olivero, L.T. Furcht, Invest. Ophthalmol. Vis. Sci. **34**, 2825 (1993)
3. G.R. Martin, R. Timpl, Annu. Rev. Cell Biol. **3**, 57 (1987). doi:10.1146/annurev.cb.03.110187.000421
4. D. Gospodarowicz, G. Greenburg, J.M. Foidart, N. Savion, J. Cell Physiol. **107**, 171 (1981). doi:10.1002/jcp.1041070203
5. G.A. Abrams, S.L. Goodman, P.F. Nealey, M. Franco, C.J. Murphy, Cell Tissue Res. **299**, 39 (2000). doi:10.1007/s004410050004
6. R.O. Hynes, Cell **69**, 11 (1992). doi:10.1016/0092-8674(92)90115-S
7. J.G. Steele, B.A. Dalton, G. Johnson, P.A. Underwood, Biomaterials **16**, 1057 (1995). doi:10.1016/0142-9612(95)98901-P
8. J.G. Steele, G. Johnson, C. Mcfarland, B.A. Dalton, T.R. Gengenbach, R.C. Chatelier, P.A. Underwood, H.J. Griesser, J. Biomater. Sci. Polym. Ed. **6**, 511 (1994). doi:10.1163/156856294X00473
9. B. Geiger, A. Bershadsky, R. Pankov, K.M. Yamada, Nat. Rev. **2**, 793 (2001)
10. V. Petit, J.P. Thiery, Biol. Cell **92**, 477 (2000). doi:10.1016/S0248-4900(00)01101-1
11. P. Clark, P. Connolly, A.S. Curtis, J.A. Dow, C.D. Wilkinson, Development **108**, 635 (1990)
12. S.-T. Li, in *The biomedical engineering handbook*, ed. by J.D. Bronzino (CRC Press Inc, Boca Raton, FL, 1995), p. 627
13. N. Matsumoto, S. Horibe, N. Nakamura, T. Senda, K. Shino, T. Ochi, Arch. Orthop. Trauma Surg. **117**, 215 (1998). doi:10.1007/s004020050232
14. P. Weiss, Growth **5**(suppl), 163 (1941)
15. A.S.G. Curtis, C.D. Wilkinson, J. Biomater. Sci. Polym. Ed. **9**, 1313 (1998). doi:10.1163/156856298X00415
16. P. Clark, P. Connolly, A.S. Curtis, J.A. Dow, C.D. Wilkinson, Development **99**, 439 (1987)
17. D.M. Brunette, Exp. Cell Res. **167**, 203 (1986). doi:10.1016/0014-4827(86)90217-X
18. A.I. Teixeira, P.F. Nealey, C.J. Murphy, J. Biomed. Mater. Res. A **71**, 369 (2004). doi:10.1002/jbm.a.30089
19. B. Wojciak-Stothard, A. Curtis, W. Monaghan, K. MacDonald, C. Wilkinson, Exp. Cell Res. **223**, 426 (1996). doi:10.1006/excr.1996.0098
20. A.I. Teixeira, G.A. Abrams, P.J. Bertics, C.J. Murphy, P.F. Nealey, J. Cell Sci. **116**, 1881 (2003). doi:10.1242/jcs.00383
21. J.Y. Yang, Y.C. Ting, J.Y. Lai, H.L. Liu, H.W. Fang, W.B. Tsai (2008) J. Biomed. Mater. Res. A. doi:10.1002/jbm.a.32130
22. R.O. Hynes, Sci. Am. **254**, 42 (1986)
23. W. Kern, D.A. Puotinen, RCA Rev **31**, 187 (1970)
24. W.B. Tsai, T.A. Horbett, J. Biomater. Sci. Polym. Ed. **10**, 163 (1999). doi:10.1163/156856299X00117
25. M.J. Dalby, M.O. Riehle, S.J. Yarwood, C.D. Wilkinson, A.S. Curtis, Exp. Cell Res. **284**, 274 (2003). doi:10.1016/S0014-4827(02)00053-8
26. A.S.G. Curtis, in *Biomechanics and cells*, ed. by F. Fyall, A.J. El (Cambridge University Press, Cambridge, 1994), p. 121
27. G.A. Dunn, A.F. Brown, J. Cell Sci. **83**, 313 (1986)
28. C.D.W. Wilkinson, M. Riehle, M. Wood, J. Gallagher, A.S.G. Curtis, Mater. Sci. Eng. C **19**, 263 (2002)
29. E.T. den Braber, J.E. de Ruijter, L.A. Ginsel, A.F. von Recum, J.A. Jansen, Biomaterials **17**, 2037 (1996). doi:10.1016/0142-9612(96)00032-4
30. X.F. Walboomers, W. Monaghan, A.S. Curtis, J.A. Jansen, J. Biomed. Mater. Res. **46**, 212 (1999). doi:10.1002/(SICI)1097-4636(199908)46:2<212::AID-JBM10>3.0.CO;2-Y
31. B. Wojciak-Stothard, A.S. Curtis, W. Monaghan, M. McGrath, I. Sommer, C.D. Wilkinson, Cell Motil. Cytoskeleton **31**, 147 (1995). doi:10.1002/cm.970310207
32. N.Q. Balaban, U.S. Schwarz, D. Riveline, P. Goichberg, G. Tzur, I. Sabanay, D. Mahalu, S. Safran, A. Bershadsky, L. Addadi, B. Geiger, Nat. Cell Biol. **3**, 466 (2001). doi:10.1038/35074532
33. X.F. Walboomers, L.A. Ginsel, J.A. Jansen, J. Biomed. Mater. Res. **51**, 529 (2000). doi:10.1002/1097-4636(20000905)51:3<529::AID-JBM30>3.0.CO;2-R
34. P.T. Ohara, R.C. Buck, Exp. Cell Res. **121**, 235 (1979). doi:10.1016/0014-4827(79)90002-8